NASA Technical Memorandum 4439

# Subsonic Aerodynamic Characteristics of a Proposed Advanced Manned Launch System Orbiter Configuration

George M. Ware and Charles H. Fox, Jr.

FEBRUARY 1993

NASA Technical Memorandum 4439

# Subsonic Aerodynamic Characteristics of a Proposed Advanced Manned Launch System Orbiter Configuration

George M. Ware and Charles H. Fox, Jr.
*Langley Research Center*
*Hampton, Virginia*

## Abstract

*The Advanced Manned Launch System is a proposed near-term technology, two-stage, fully reusable launch system that consists of an unmanned glide-back booster and a manned orbiter. An orbiter model that featured a large fuselage and an aft delta wing with tip fins was tested in the Langley 7- by 10-Foot High-Speed Tunnel. A crew cabin, large payload fairing, and crew access tunnel were mounted on the upper body. The results of the investigation indicated that the configuration was longitudinally stable to an angle of attack of about 6° about a center-of-gravity position of 0.7 body length. The model had an untrimmed lift-drag ratio of 6.6, but could not be trimmed at positive lift. The orbiter model was also directionally unstable. The payload fairing was responsible for about half the instability. The tip-fin controllers, which are designed as active controls to produce artificial directional stability, were effective in producing yawing moment, but sizable adverse rolling moment occurred at angles of attack above 6°. Differential deflection of the elevon surfaces was effective in producing rolling moment with only small values of adverse yawing moment.*


## Introduction

The National Aeronautics and Space Administration is investigating several concepts for future space transportation systems (refs. 1–9), one of which is a two-stage system designed as a near-term technology, fully reusable Advanced Manned Launch System (AMLS). It consists of an unmanned glide-back booster and a manned orbiter. Both elements are similar body-delta wing designs. The orbiter is mounted over the booster such that the engines of each element are in the same plane. The AMLS is vertically launched with all engines thrusting. Fuel is crossfed from the booster to the orbiter so that, at separation (Mach number of 3), the orbiter has full tanks. The booster glides back to the launch site (ref. 10) and makes a horizontal landing. The orbiter continues on to orbit under its own power. After completing the mission, the orbiter returns to Earth as an unpowered glider much like the Space Shuttle orbiter does.

The present investigation was made to determine the subsonic aerodynamic characteristics of the AMLS orbiter during unpowered entry. The orbiter has a large fuselage for fuel tanks and engines. A movable body flap extends aft of the fuselage. A delta wing is mounted far aft on the lower body and is equipped with elevon surfaces and tip fins. The crew cabin, payload compartment, and access tunnel from the crew area to the payload bay are mounted on the upper body. The test was conducted in the Langley 7- by 10-Foot High-Speed Tunnel (7- by 10-Foot Tunnel).

## Symbols

The longitudinal data are referred to the stability-axis system and the lateral-directional data are referred to the body-axis system (fig. 1). The data are normalized by the planform area and span of the wing and by the length of the body, excluding the body flap. The moment reference center was located at the proposed vehicle center of gravity, which is at 0.7 body length from the nose and 1.6 percent body length above the lower surface.

| | |
|---|---|
| $b$ | body span, in. |
| $C_D$ | drag coefficient, Drag/$qS_{\text{ref}}$ |
| $C_L$ | lift coefficient, Lift/$qS_{\text{ref}}$ |
| $C_l$ | rolling moment coefficient, Rolling moment/$qS_{\text{ref}}b$ |
| $C_{l_\beta}$ | $\Delta C_l/\Delta\beta$, taken at $\beta = 0°$ and 4°, per deg |
| $C_m$ | pitching moment coefficient, Pitching moment/$qS_{\text{ref}}\ell$ |
| $C_n$ | yawing moment coefficient, Yawing moment/$qS_{\text{ref}}b$ |
| $C_{n_\beta}$ | $\Delta C_n/\Delta\beta$, taken at $\beta = 0°$ and 4°, per deg |
| $C_p$ | pressure coefficient, $(p_{\text{local}} - p_\infty)/q$ |
| $C_Y$ | side-force coefficient, Side force/$qS_{\text{ref}}$ |

| | |
|---|---|
| $C_{Y_\beta}$ | $\Delta C_Y/\Delta\beta$ taken at $\beta = 0°$ and $4°$, per deg |
| $L/D$ | lift-drag ratio |
| $\ell$ | body length, in. |
| $M$ | Mach number |
| $p$ | pressure, lb/in$^2$ |
| $q$ | free-stream dynamic pressure, lb/in$^2$ |
| $S_{\text{ref}}$ | wing planform area (excluding body flap), in$^2$ |
| $X$ | longitudinal body axis |
| $Y$ | lateral body axis |
| $Z$ | vertical body axis |
| $\alpha$ | angle of attack, deg |
| $\beta$ | angle of sideslip, deg |
| $\delta_a$ | aileron (differential pitch) control deflection angle $(\delta_{e,L} - \delta_{e,R})/2$, deg |
| $\delta_{BF}$ | body flap deflection angle (positive when deflected downward), deg |
| $\delta_e$ | elevon deflection angle (positive when deflected downward), deg |
| $\delta_{TF}$ | tip-fin controller deflection angle (positive when deflected with the trailing edge to the left), deg |

Subscripts:

| | |
|---|---|
| max | maximum value |
| $L$ | left |
| $R$ | right |
| $\infty$ | free stream |

## Description of Model

A sketch of the two-stage AMLS orbiter and glide-back booster is shown in figure 2. Only the subsonic aerodynamic characteristics of the orbiter element were studied in this investigation. A detailed sketch of the orbiter model is presented in figure 3, and a photograph of the model in the 7- by 10-Foot Tunnel is presented in figure 4. Model dimensional information is given in table I.

The aluminum model was a 1.12-percent-scale representation of a proposed 149-ft-long vehicle. The configuration consisted of a large body with a delta wing mounted on the far aft underside. A body flap extended aft from the lower body. The wing was equipped with elevon surfaces and small tip fins. The crew compartment, payload fairing, and access tunnel between the two were made of wood and mounted on the upper body. These components could be removed to assess their effect on the aerodynamic characteristics of the model. The payload fairing and body, which were boattailed in the baseline configuration, could be replaced with unboattailed units. Figure 5 presents the various model configurations tested.

The effectiveness of pitch, roll, and yaw control was tested. The pitch control investigation consisted of deflections of $-10°$ on the elevons and $-13°$ on the body flap. Roll control was accomplished by differential deflection of the elevons and yaw control by deflection of the tip-fin controller. The controller consisted of a rudder-like surface on each fin that could only be deflected outward. This surface was simulated by a 45° wooden wedge attached to the outboard left fin only (fig. 3). A unique feature of the AMLS orbiter is its far aft center of gravity. During entry with empty fuel tanks and the aft-positioned heavy rocket motors, the center of gravity is estimated at 0.7 body length.

## Apparatus, Tests, and Corrections

Tests were conducted in the 7- by 10-Foot Tunnel. The facility is a closed-circuit, subsonic atmospheric tunnel with a nominal 7-ft-high by 10-ft-wide test section. A more complete description of the facility is given in reference 11. The model was sting mounted through its base, and forces and moments were measured with an internally mounted strain-gauge balance. Model angles of attack and sideslip were corrected for sting and balance deflection under load. Customary tunnel interference corrections were applied to the data. In an attempt to ensure turbulent flow over the model, transition grit was applied in accordance with reference 12. Number 100 carborundum grit was thinly sprinkled in 1/16-in. bands 1 in. aft of the nose and 1 in. streamwise on the wings. The model test pitch range was nominally from $-2°$ to $20°$. The model was tested at angles of sideslip of $0°$ and $4°$ over the range. Data were taken as the model was moved from negative to positive angles. Base pressures on the boattailed and unboattailed fuselage base, unboattailed payload fairing, and model balance cavity were measured and are presented as figure 6 if base corrections are desired.

## Results and Discussion

The data were measured at Mach numbers of 0.3 and 0.6. For clarity, the following discussion will center on the data for $M_\infty = 0.3$. When the data for $M_\infty = 0.6$ differ significantly from the data for $M_\infty = 0.3$, the difference will be noted.

### Longitudinal Characteristics

***Effects of payload fairing.*** The most prominent feature of the AMLS orbiter configuration is the large external payload fairing on the upper fuselage. The primary interest was to determine the effect of this fairing on the aerodynamic characteristics of the model. Data for the model with fairing on and off are presented in figure 7. The effects are about as expected. When the payload fairing was removed, drag was reduced and the maximum $L/D$ increased from 6.6 to 7.7. Because the fairing was above the vertical center of gravity, fairing drag also produced a nose-up pitching moment increment. The model was longitudinally stable at low angles of attack, even with the center of gravity at 0.7 body length. This stability is attributable to the far aft wing location. At about $\alpha = 6°$, the pitching moment lost linearity and the configuration with or without fairing became longitudinally unstable. The model had a large value of negative pitching moment at $C_L = 0$ that occurs at about $\alpha = -4°$ (extrapolated). As a result, the configuration with controls undeflected has no stable trim condition in the positive lift range. The lift curve slope is linear to about $\alpha = 6°$ before showing signs of flow separation. At $M_\infty = 0.6$, the flow separation is aggravated and lift becomes nonlinear at somewhat lower angles of attack.

***Effects of boattails.*** The baseline AMLS orbiter design incorporates boattailed aft sections on both the payload fairing and aft fuselage. Because of length constraints, the boattail angles are quite severe. A concern that the airflow would separate at the boattails and that the effectiveness in reducing base drag would be lost did not materialize; the data of figure 8 indicate that the boattails were effective. When the boattails were removed and replaced with unboattailed sections, drag increased and a loss in $(L/D)_{\max}$ resulted. The maximum untrimmed lift-drag ratio was reduced from 6.6 to 5.9 when the body boattail was removed and to 5.2 when both boattails were removed. The shape of the body boattail simulated a downward-deflected control surface. The effect of this shape is reflected in the pitching moment curve. When the boattail was removed, the curve shifted in a positive direction. The boattail, which was beneficial in increasing the untrimmed $L/D$ ratio, had an adverse effect on pitching moment; that is, the pitching moment curve shifted in a negative direction that placed the configuration in a condition that was more out of trim. The data show that removal of the payload-fairing boattail had little effect on pitching moment.

The effects of the body boattail with the payload fairing removed were also investigated; those data are presented in figure 9. Again, the powerful effect of the body boattail on pitching moment is noted. Pitching moment shifted in a positive direction that is less out of trim when the boattail is removed. The addition of a boattail to the body (with payload fairing removed) resulted in a gain in untrimmed $L/D$ of about 1.5.

***Pitch control characteristics.*** The characteristics are presented in figure 10 for the baseline AMLS model with elevons and body flap deflected as pitch controls. Elevon deflection of $-10°$ was effective in shifting the pitching moment curve in the positive direction. The model, however, was still far out of positive longitudinal trim. When $-13°$ body flap deflection was added to elevon deflection, the model trimmed at $\alpha = -2°$, where the lift value was slightly negative. The controls as configured will likely be incapable of trimming the AMLS orbiter for successful subsonic flight and landing. If positive longitudinal stability is not a design requirement (as suggested in refs. 13 and 14), then a smaller wing is indicated. However, a smaller wing (with the same center-of-pressure location) would have a destabilizing effect and unstable trim would result at positive lift values. The orbiter would then require artificial pitch stabilization. Therefore, the longitudinal aerodynamic characteristics of the orbiter suggest that some configuration modifications will be necessary.

### Lateral Characteristics

***Lateral-directional stability.*** The lateral-directional characteristics of the AMLS orbiter are presented in figure 11 in the form of stability parameters $C_{Y_\beta}$, $C_{n_\beta}$, and $C_{l_\beta}$ plotted against angle of attack. Data are shown for the model with and without payload fairing. The tip fins were not designed to stabilize the configuration, but are used to house an active control that adds artificial stability. (See refs. 13–15 for a description of tip-fin controllers and their use.) The baseline AMLS is directionally unstable (negative values of $C_{n_\beta}$) and has low values of positive effective dihedral (negative values of $C_{l_\beta}$) for most of the $\alpha$ range. The payload fairing is directionally destabilizing. Removal of the fairing reduces the directional instability to about half its original value. The fairing has only a small effect on

values of $C_{l_\beta}$. Removal of the boattails on the payload fairing and body (fig. 12) had little effect on the lateral-directional characteristics of the model.

***Yaw control effects.*** All lateral control tests were made with the baseline configuration. Yaw control was accomplished by the outward deflection of the controller surface on one tip fin. The tip-fin controller produces yawing moment primarily through increased drag at the wing tip. The data of figure 13 indicate that the controller was effective. Yawing moment to the left resulted from left controller deflection ($\delta_{TF} = 45°$) and decreased only slightly over the $\alpha$ range. Controller deflection, however, resulted in larger rolling moments than yawing moments above an $\alpha$ of about 8°. That large rolling moment is explained in reference 16, in which oil flow studies showed a deflected tip-fin controller to delay flow separation. On the wing with an undeflected controller, flow separation occurred at the wing tip inside the tip fin. The resulting unbalanced lift between the wings with deflected and undeflected controllers produced the large rolling moment. This adverse rolling moment poses a serious problem for lateral-directional control.

***Roll control effects.*** Roll control was accomplished through a differential deflection of the elevons. The effectiveness values are for cases with the left elevon set at $-10°$ while the right control remained at 0°. This deflection represents $-5°$ of aileron deflection $\delta_a$ about a pitch setting of $-5°$. The data of figure 14 indicate that the elevons were relatively effective for roll control. The surfaces produced only small values of adverse yawing moment.

## Concluding Remarks

Tests of a proposed two-stage Advanced Manned Launch System (AMLS) orbiter configuration have been conducted in the Langley 7- by 10-Foot High-Speed Tunnel to study the subsonic aerodynamic characteristics of the orbiter during gliding entry. The model had a large fuselage and an aft delta wing with tip fins. A crew cabin, payload fairing, and crew access tunnel were mounted on the upper body. The results of the investigation indicated that the configuration was longitudinally stable to an angle of attack of approximately 6° about a center-of-gravity position of 0.7 body length. Although the untrimmed lift-drag ratio was relatively high for a spacecraft (6.6), the configuration could not be trimmed with positive longitudinal stability at positive lift. With $-10°$ elevon and $-13°$ body flap deflection available for the test, the model was trimmed at an angle of attack of $-2°$. Configuration modifications will be necessary to improve vehicle trim capability. The boattailed aft sections of the payload fairing and body were effective in improving the subsonic lift-drag ratio. The body boattail, however, aggravated the negative pitching moment problem. When the external payload fairing was removed, the untrimmed lift-drag value increased by about 1.5.

The orbiter was directionally unstable. The payload fairing was responsible for about half the instability. The directional control results from deflection of the tip-fin controllers. The controllers were effective in producing yawing moment, but very large adverse rolling moments occurred at angles of attack above 8°. Roll control is accomplished by conventional elevon surfaces. These surfaces were effective, and only small values of adverse yawing moment resulted.

NASA Langley Research Center
Hampton, VA 23681-0001
December 22, 1992

## References

1. Freeman, Delma C., Jr.: The New Space Transportation Begins Today. *Astronaut. & Aeronaut.,* vol. 21, no. 6, June 1983, pp. 36–37, 48.

2. Martin, James A.: Orbit on Demand: In This Century If Pushed. *Aerosp. America,* vol. 23, no. 2, Feb. 1985, pp. 46–48.

3. Talay, T. A.: Shuttle II. SAE Tech. Paper Ser. 871335, June 1987.

4. Holloway, Paul F.; and Talay, Theodore A.: Space Transportation Systems—Beyond 2000. IAF Paper 87-188, Oct. 1987.

5. Talay, Theodore A.; and Morris, W. Douglas: Advanced Manned Launch Systems. Paper presented at AAAF, DGLR, Royal Aeronautical Society, and ESA Second European Aerospace Conference on Progress in Space Transportation (Bonn, Federal Republic of Germany), May 22–24, 1989.

6. Freeman, Delma C.; Talay, Theodore A.; Stanley, Douglas O.; and Wilhite, Alan W.: Design Options for Advanced Manned Launch Systems (AMLS). AIAA-90-3816, Sept. 1990.

7. Freeman, Delma C., Jr.; Wilhite, Alan W.; and Talay, Theodore A.: Advanced Manned Launch System Study Status. IAF Paper 91-193, Oct. 1991.

8. Ehrlich, C. F., Jr.; and Stone, H. W., Jr.: Space Transportation System Design for Operations in the 2000+ Era. IAF Paper 92-0880, Aug.–Sept. 1992.

9. Stone, H. W.; and Piland, W. M.: An Advanced Manned Launch System Concept. IAF Paper 92-0870, Aug.–Sept. 1992.

10. Naftel, J. C.; and Powell, R. W.: Aerodynamic Separation and Glideback of a Mach 3 Staged Booster. AIAA-90-0223, Jan. 1990.

11. Peñaranda, Frank E.; and Freda, M. Shannon: *Aeronautical Facilities Catalogue. Volume 1—Wind Tunnels.* NASA RP-1132, 1985.

12. Braslow, Albert L.; Hicks, Raymond M.; and Harris, Roy V., Jr.: Use of Grit-Type Boundary-Layer-Transition Trips. *Conference on Aircraft Aerodynamics,* NASA SP-124, 1966, pp. 19–36.

13. Freeman, Delma C., Jr.; and Wilhite, Alan W.: *Effects of Relaxed Static Longitudinal Stability on a Single-Stage-to-Orbit Vehicle Design.* NASA TP-1594, 1979.

14. Freeman, Delma C., Jr.; and Powell, Richard W.: Impact of Far-Aft Center of Gravity for a Single-Stage-to-Orbit Vehicle. *J. Spacecr. & Rockets,* vol. 17, no. 4, July–Aug. 1980, pp. 311–315.

15. Powell, Richard W.; and Freeman, Delma C., Jr.: Application of a Tip-Fin Controller to the Shuttle Orbiter for Improved Yaw Control. AIAA-81-0074, Jan. 1981.

16. Lepsch, R. A., Jr.; and MacConochie, I. O.: Subsonic Aerodynamic Characteristics of a Circular Body Earth-to-Orbit Transport. AIAA-86-1801, June 1986.

Table I. Geometric Characteristics of AMLS Orbiter Model

| | |
|---|---|
| **Body:** | |
| Length (reference length), in. | 20.00 |
| Maximum width, in. | 4.80 |
| Maximum height (excluding payload fairing), in. | 3.25 |
| Maximum height (including payload fairing), in. | 5.38 |
| Base area (boattailed), $in^2$ | 11.50 |
| Base area (unboattailed), $in^2$ | 14.30 |
| Payload fairing base area (unboattailed), $in^2$ | 1.87 |
| Balance cavity area, $in^2$ | 3.97 |
| **Wing:** | |
| Airfoil | NACA 0010-10 |
| Incidence, deg | 1.5 |
| Dihedral, deg | 7.0 |
| Washout, deg | 3.0 |
| Sweep, deg | 45.0 |
| Span (reference span), in. | 15.14 |
| Chord (body centerline), in. | 9.30 |
| Chord (body-wing intersection), in. | 6.90 |
| Chord (tip), in. | 1.72 |
| Area (to body centerline, reference area), $in^2$ | 83.42 |
| Area (exposed), $in^2$ | 44.56 |
| **Tip fins (each):** | |
| Airfoil | NACA 0010-10 |
| Span (in plane of fin), in. | 1.30 |
| Chord (tip), in. | 0.43 |
| Chord (root), in. | 1.73 |
| Rollout (from vertical), deg | 10.00 |
| Area, $in^2$ | 1.40 |
| **Elevons (each):** | |
| Span, in. | 3.72 |
| Chord, in. | 1.20 |
| Area, $in^2$ | 4.46 |
| **Body flap:** | |
| Span (tip), in. | 4.31 |
| Span (root), in. | 4.80 |
| Chord, in. | 0.95 |
| Area, $in^2$ | 4.33 |
| **Tip-fin controllers (each):** | |
| Span, in. | 1.30 |
| Chord (tip), in. | 0.43 |
| Chord (root), in. | 0.93 |
| Area, $in^2$ | 0.88 |

Figure 1. System of axes with positive directions of forces, moments, velocities, and angles.

Figure 2. Proposed two-stage Advanced Manned Launch System.

Figure 3. Model used in investigation. All linear dimensions are in inches.

L-92-09038

Figure 4. The AMLS orbiter model mounted in the Langley 7- by 10-Foot Tunnel.

Figure 5. Model configurations.

(a) $M_\infty = 0.3$.

(b) $M_\infty = 0.6$.

Figure 6. Typical model base and chamber pressures.

(a) $M_\infty = 0.3$.

Figure 7. Effect of payload fairing on longitudinal aerodynamic characteristics of AMLS orbiter.

(b) $M_\infty = 0.6$.

Figure 7. Concluded.

(a) $M_\infty = 0.3$.

Figure 8. Effect of boattails on longitudinal aerodynamic characteristics of AMLS orbiter.

(b) $M_\infty = 0.6$.

Figure 8. Concluded.

(a) $M_\infty = 0.3$.

Figure 9. Effect of body boattail on longitudinal aerodynamic characteristics of AMLS orbiter. Payload fairing off.

(b) $M_\infty = 0.6$.

Figure 9. Concluded.

(a) $M_\infty = 0.3$.

Figure 10. Effect of pitch control deflection on longitudinal aerodynamic characteristics of AMLS orbiter.

(b) $M_\infty = 0.6$.

Figure 10. Concluded.

(a) $M_\infty = 0.3$.

Figure 11. Effect of payload fairing on lateral-directional aerodynamic characteristics of AMLS orbiter.

(b) $M_\infty = 0.6$.

Figure 11. Concluded.

(a) $M_\infty = 0.3$.

Figure 12. Effect of boattails on lateral-directional aerodynamic characteristics of AMLS orbiter.

(b) $M_\infty = 0.6$.

Figure 12. Concluded.

(a) $M_\infty = 0.3$.

Figure 13. Effect of yaw control deflection on lateral-directional aerodynamic characteristics of AMLS orbiter.

(b) $M_\infty = 0.6$.

Figure 13. Concluded.

(a) $M_\infty = 0.3$.

Figure 14. Effect of roll control deflection on lateral-directional aerodynamic characteristics of AMLS orbiter.

(b) $M_\infty = 0.6$.

Figure 14. Concluded.

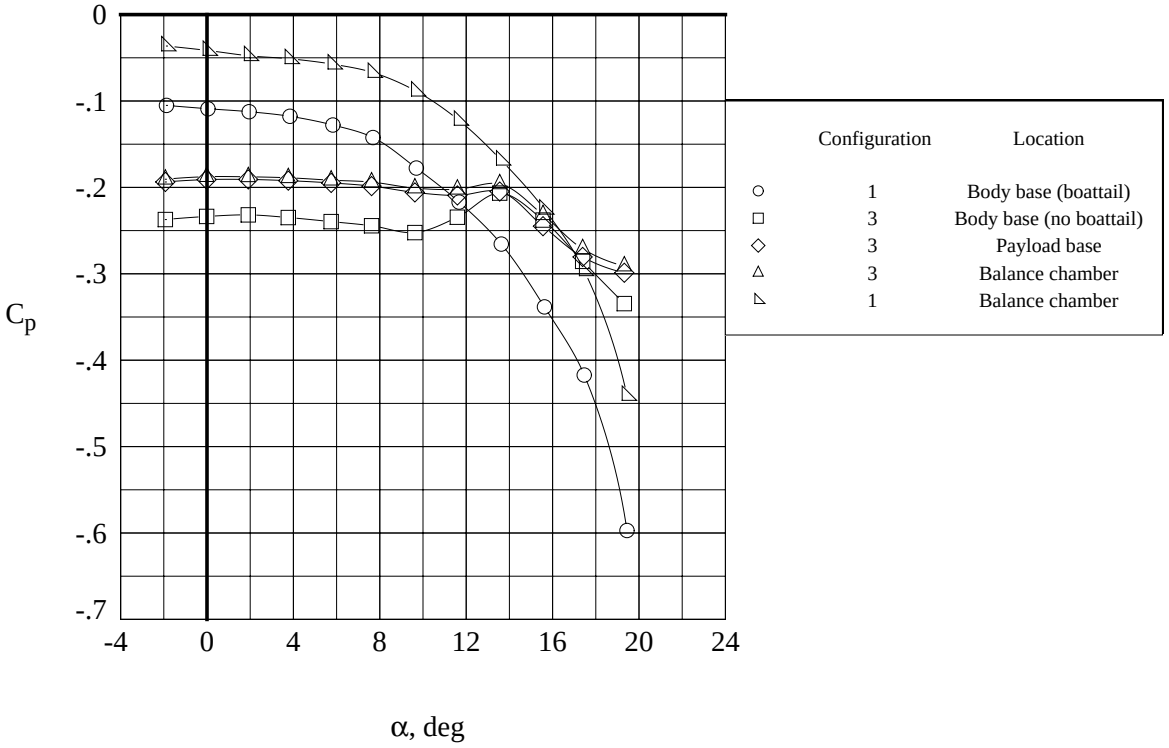


(a) $M_\infty = 0.3$

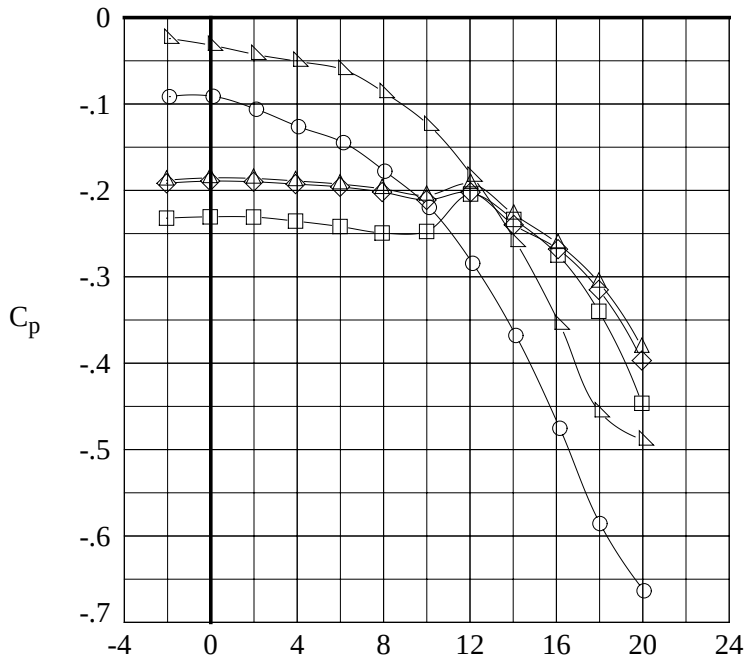


(b) $M_\infty = 0.6$

Figure 6. Typical model base and chamber pressures.

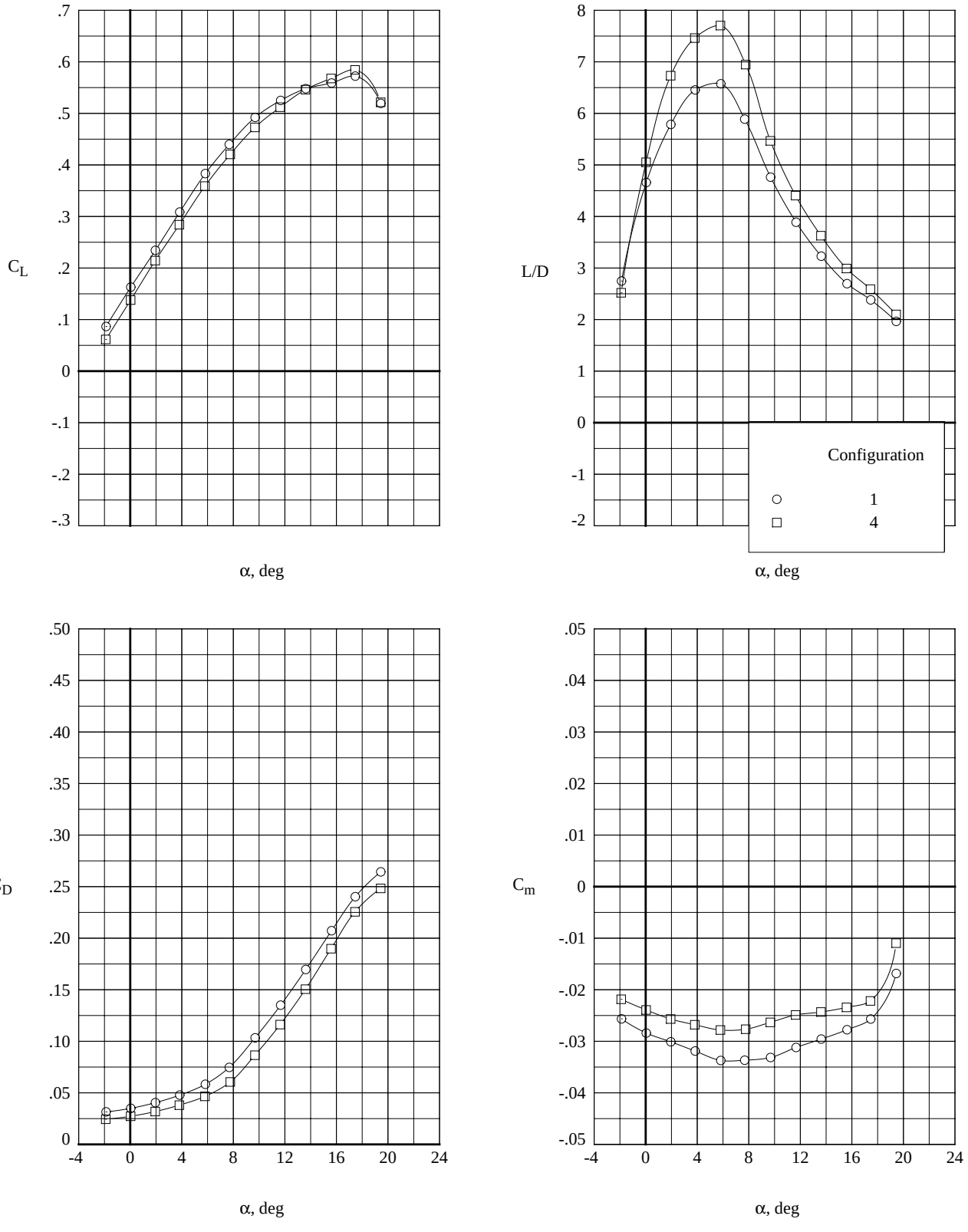


(a) M = 0.3

Figure 7. Effect of payload fairing on the longitudinal aerodynamic characteristics of the AMLS orbiter.

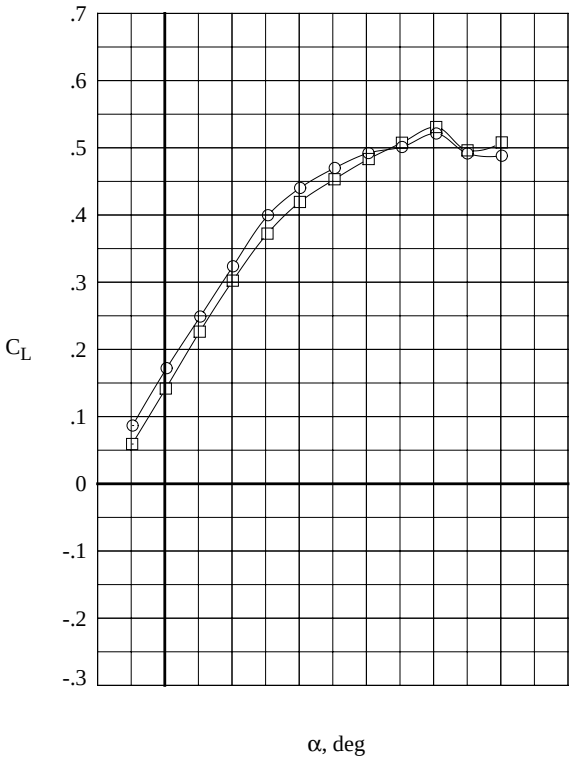


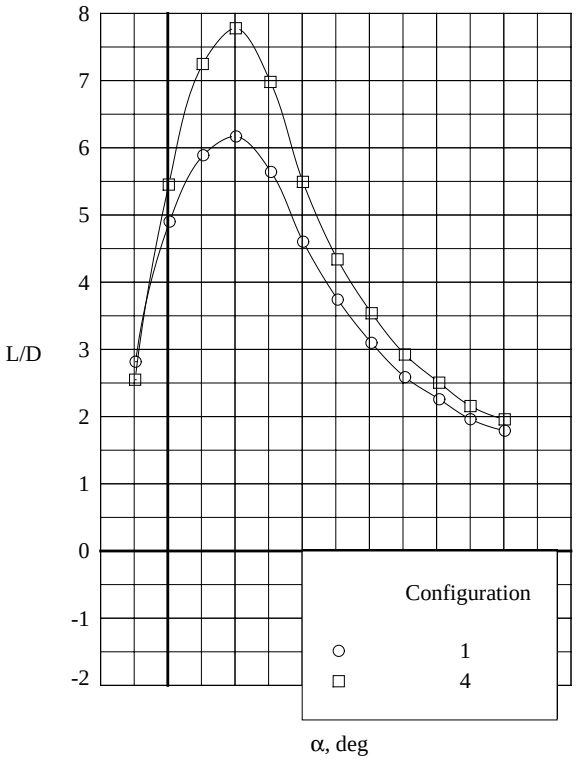


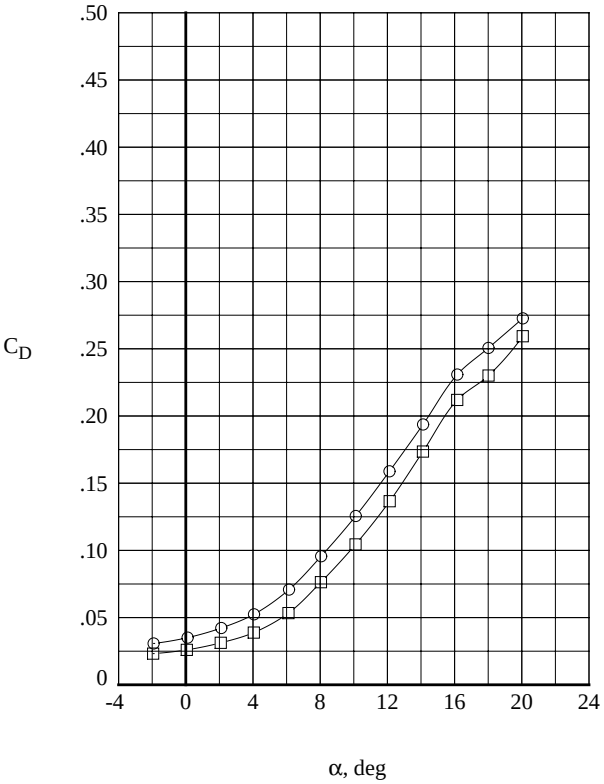


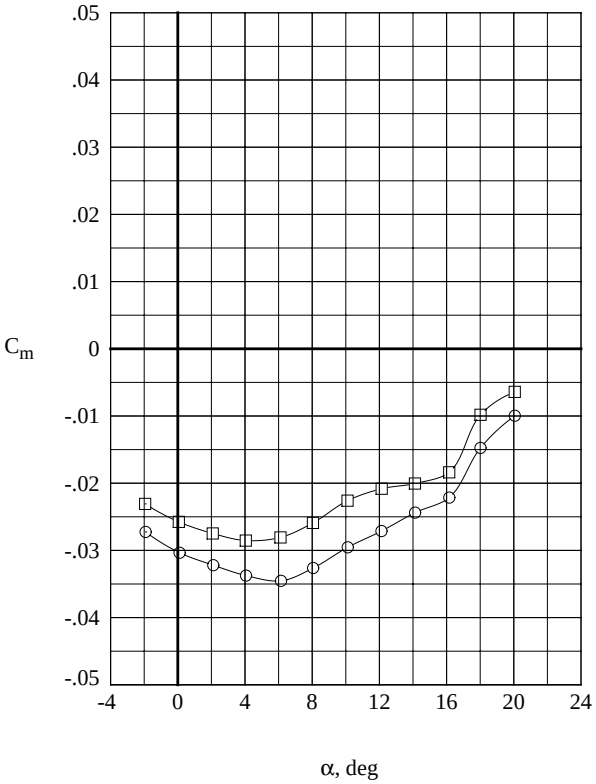


(b) M = 0.6

Figure 7. Concluded.

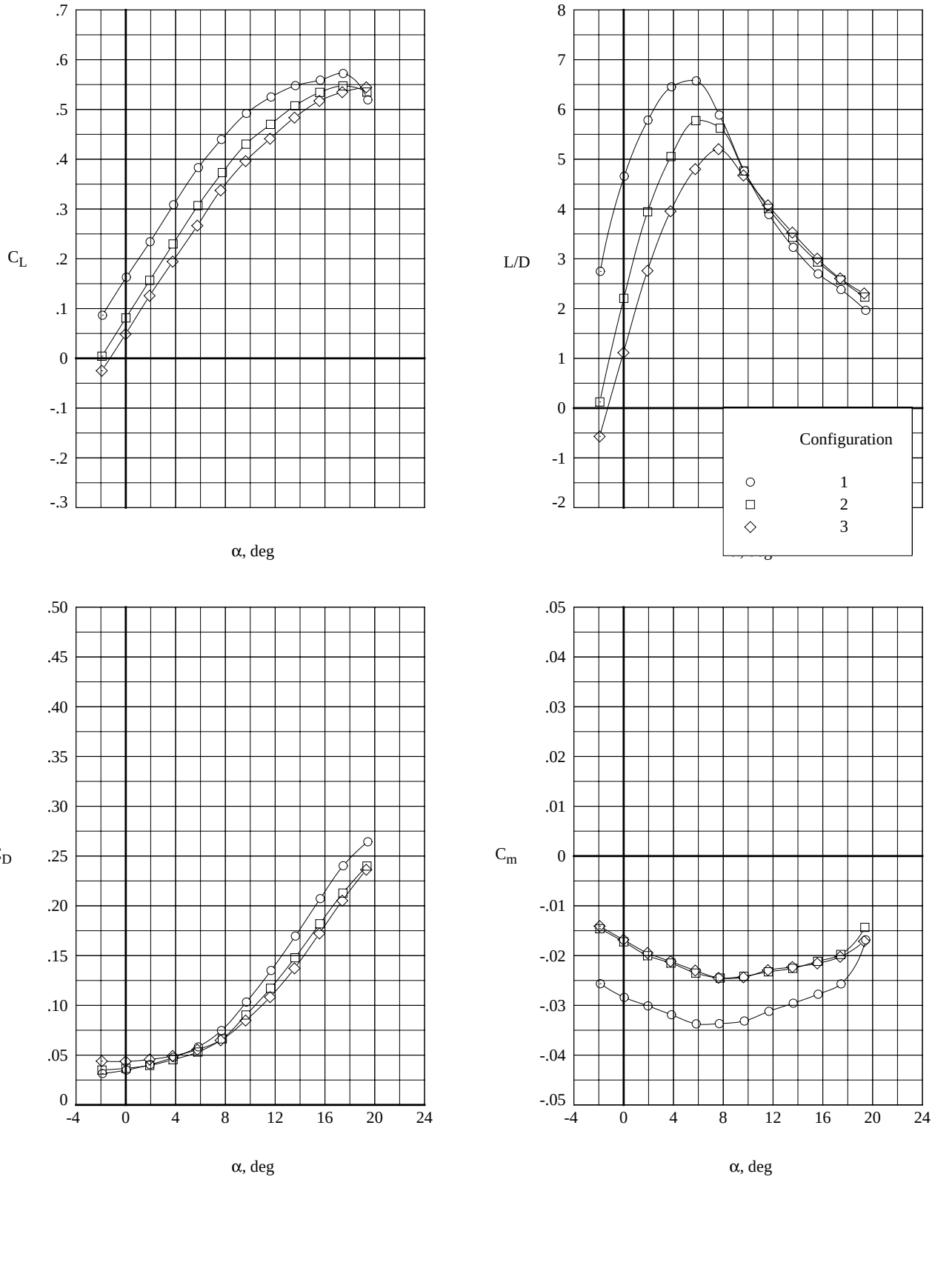


(a) M = 0.3

Figure 8. Effect of boattails on the longitudinal aerodynamic characteristics of the AMLS orbiter.

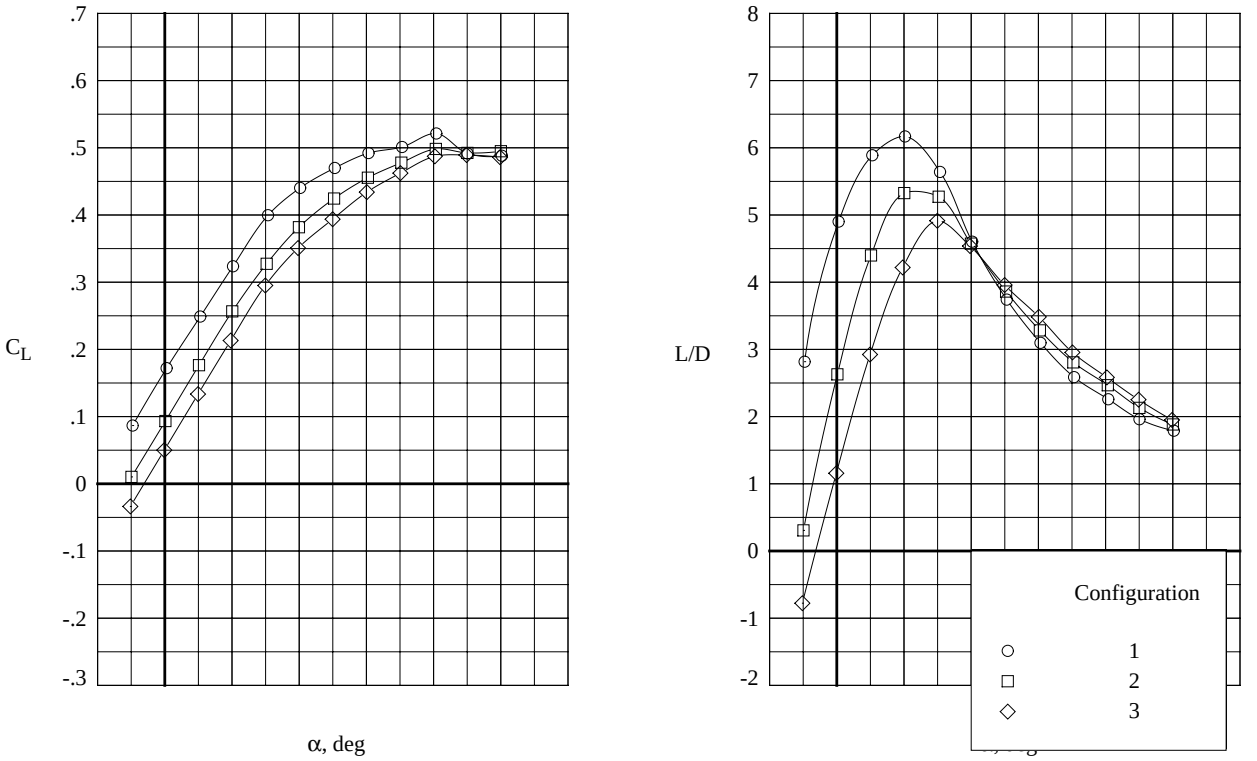


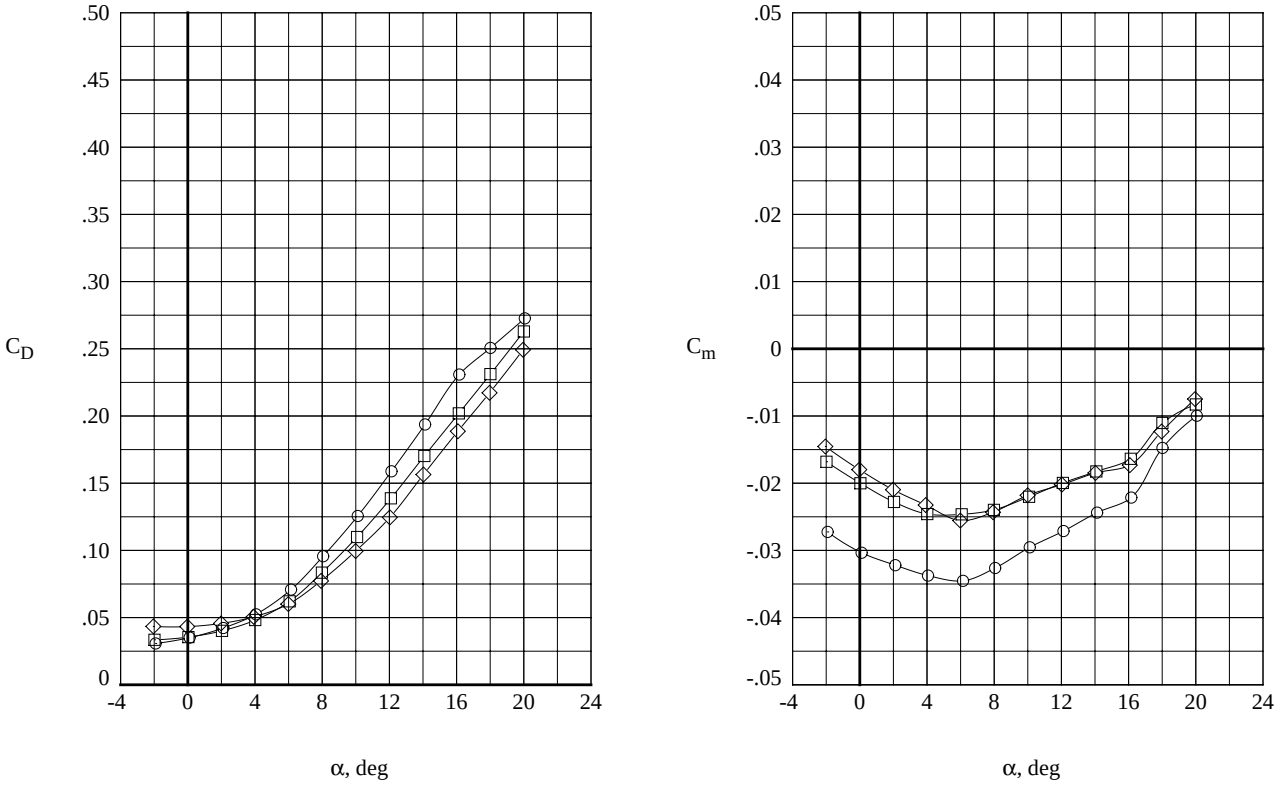


(b) M = 0.6

Figure 8. Concluded

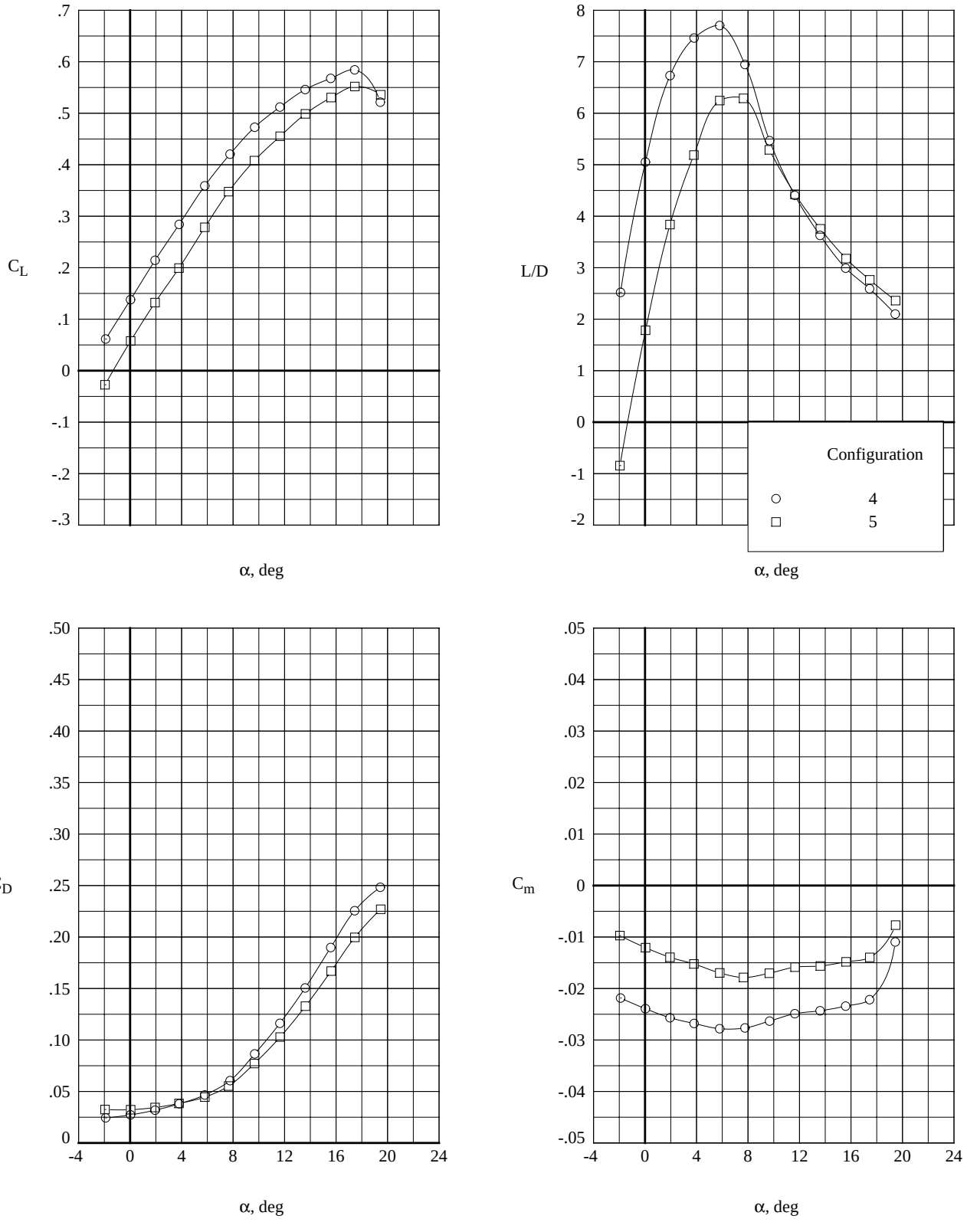


(a) M = 0.3

Figure 9. Effect of body boattail on the longitudinal aerodynamic characteristics of the AMLS orbiter. Payload fairing off.

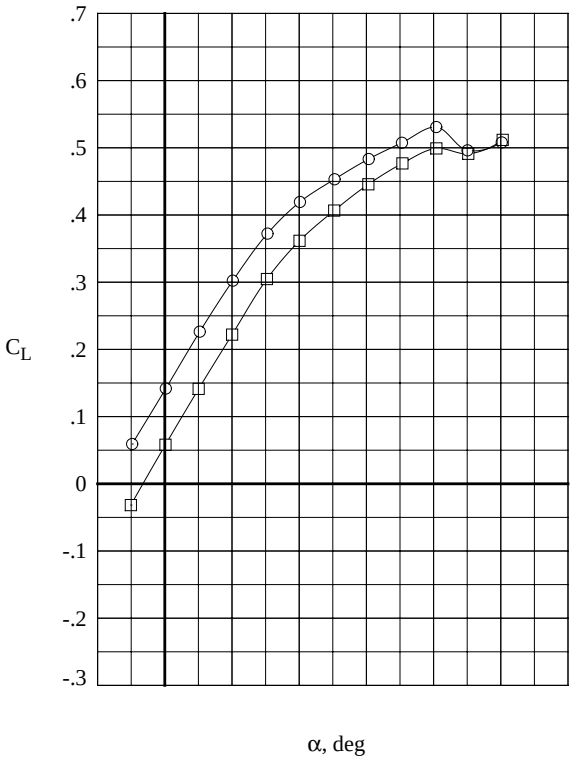


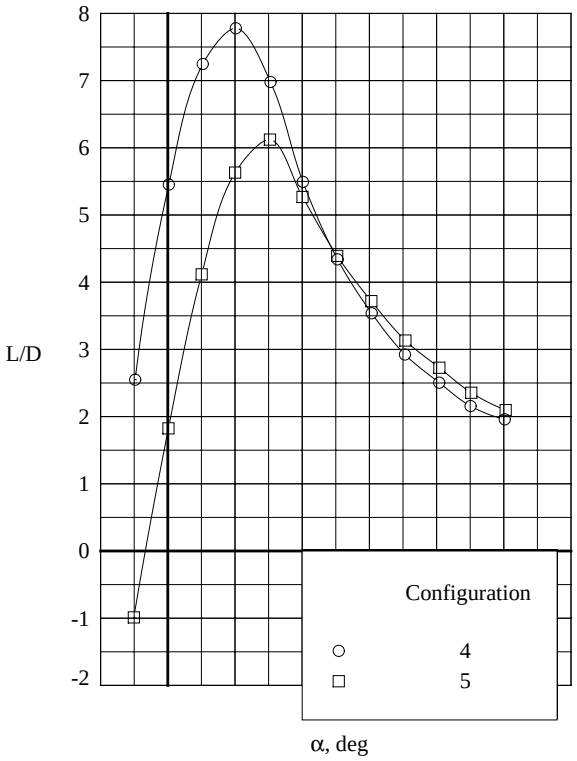


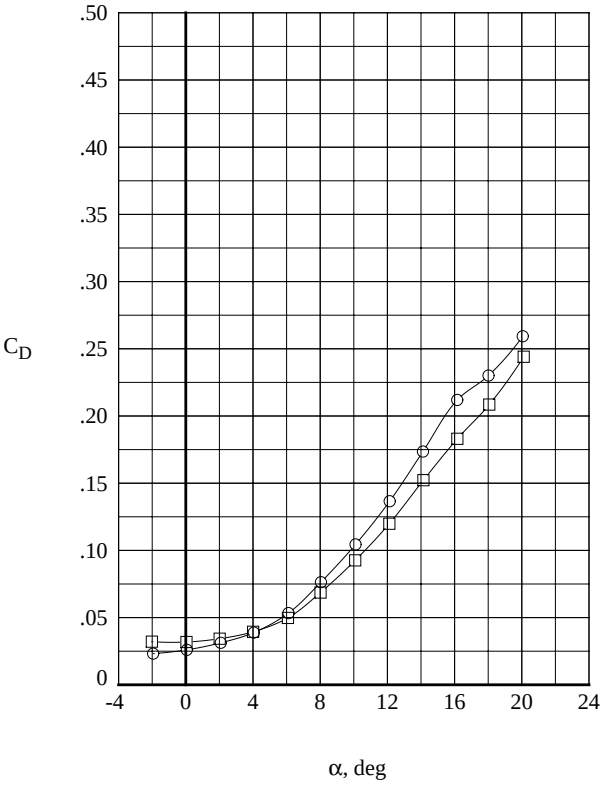


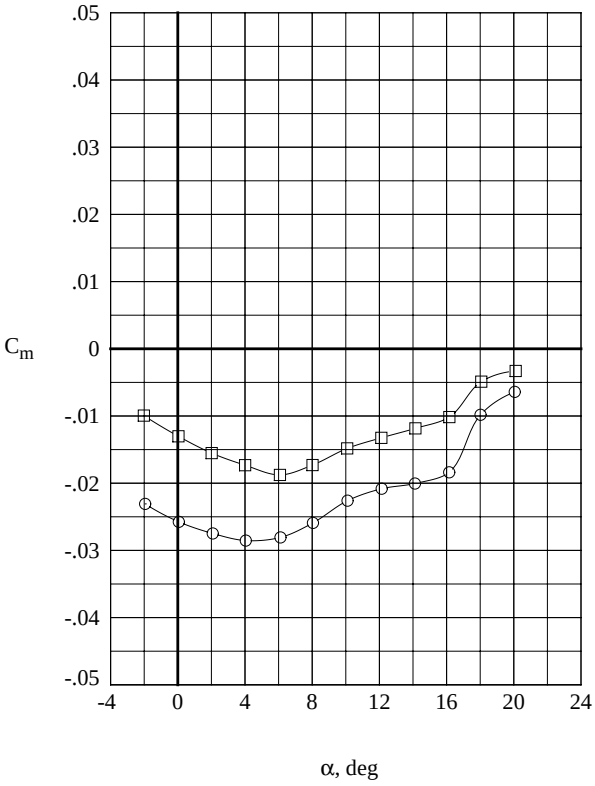


(b) M = 0.6

Figure 9. Concluded.

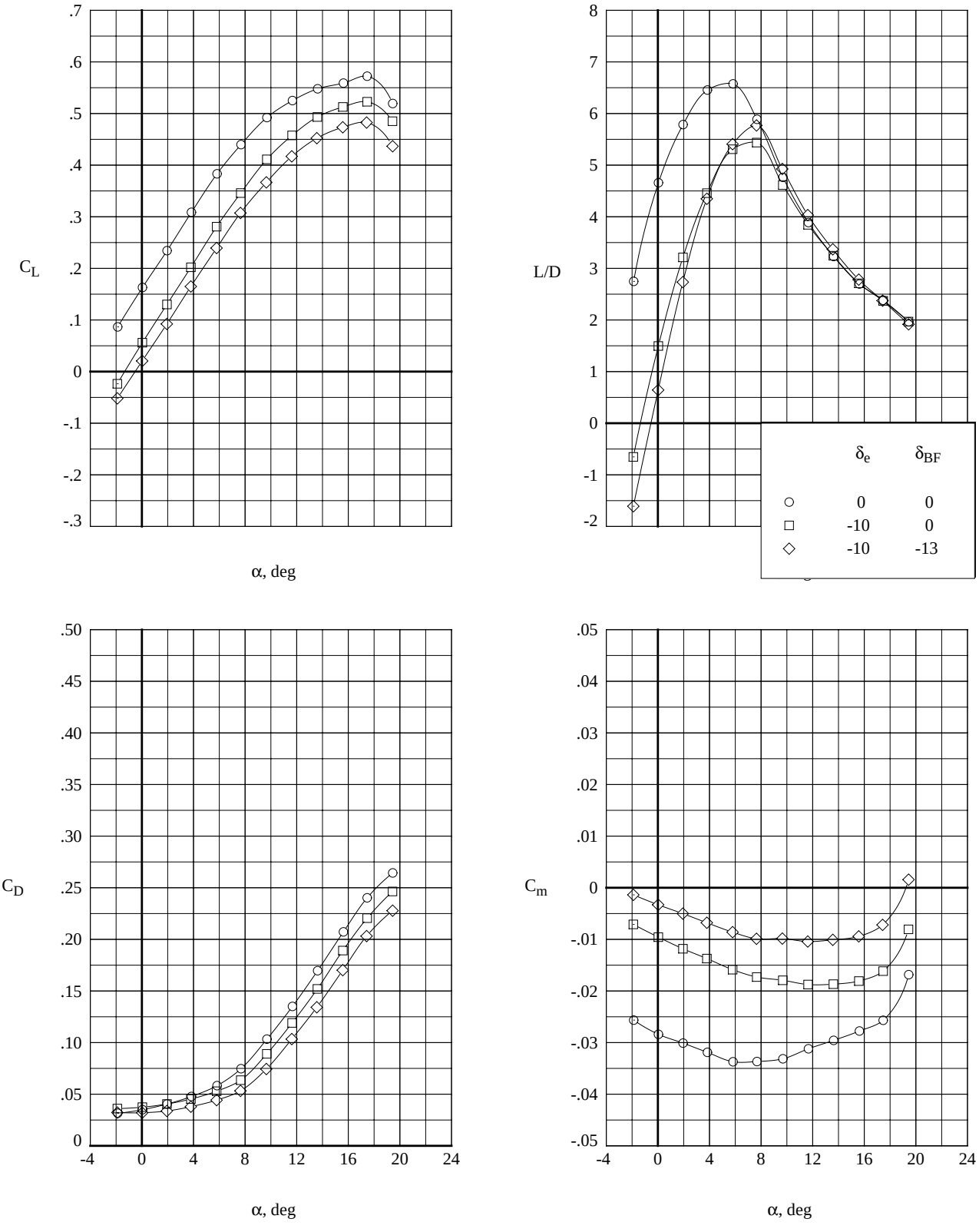


(a) M = 0.3

Figure 10. Effect of pitch control deflection on the longitudinal aerodynamic characteristic of the AMLS orbiter.

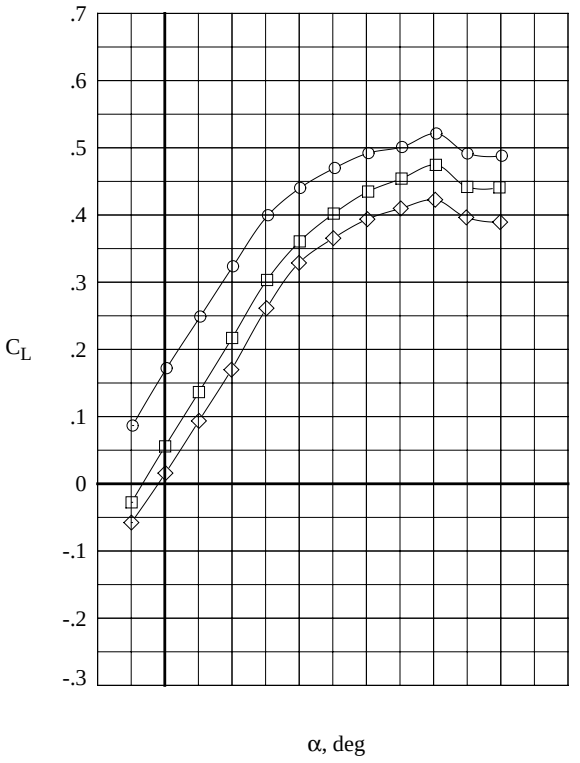


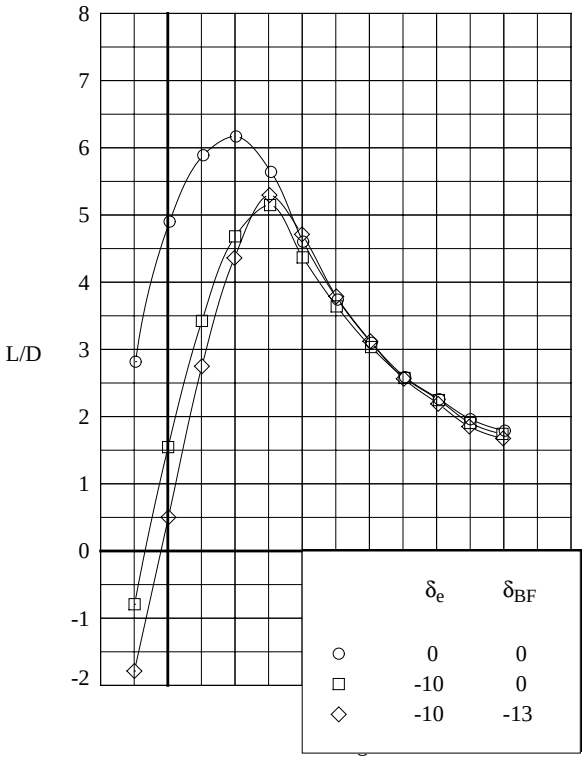


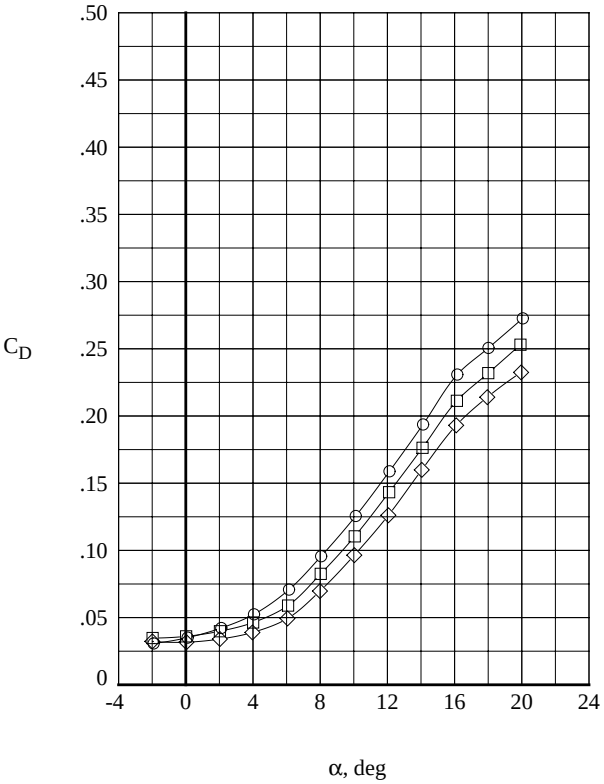


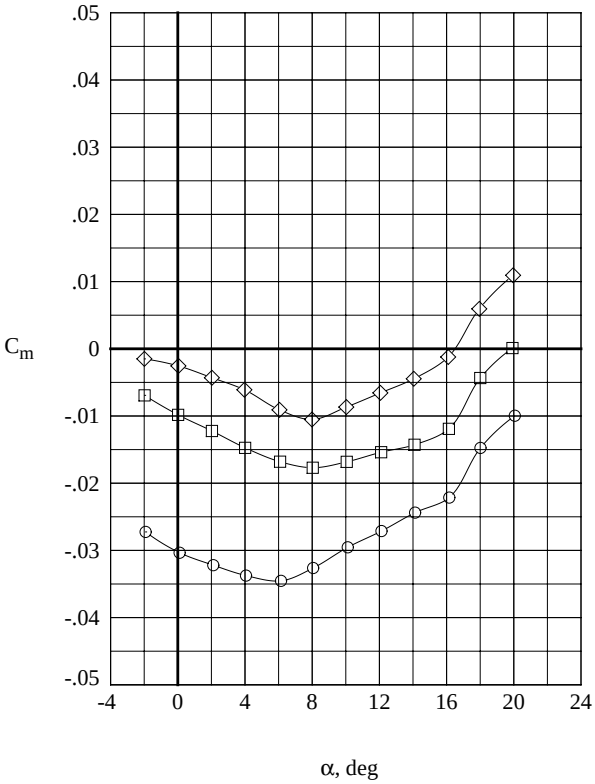


(b) M = 0.6

Figure 10. Concluded.

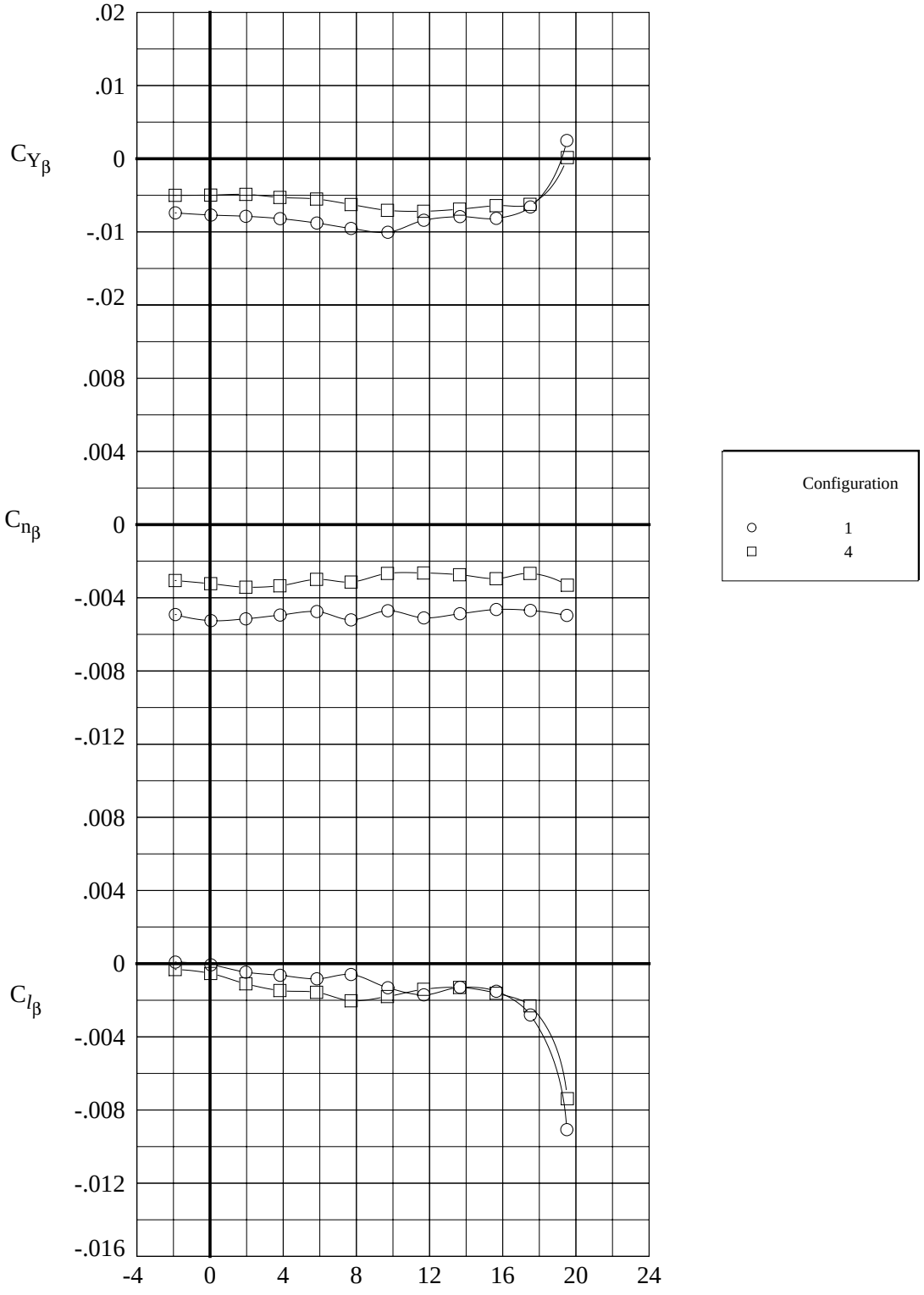


(a) $M_\infty = 0.3$

Figure 11. Effect of payload fairing on the lateral-directional aerodynamic characteristics of the AMLS orbiter.

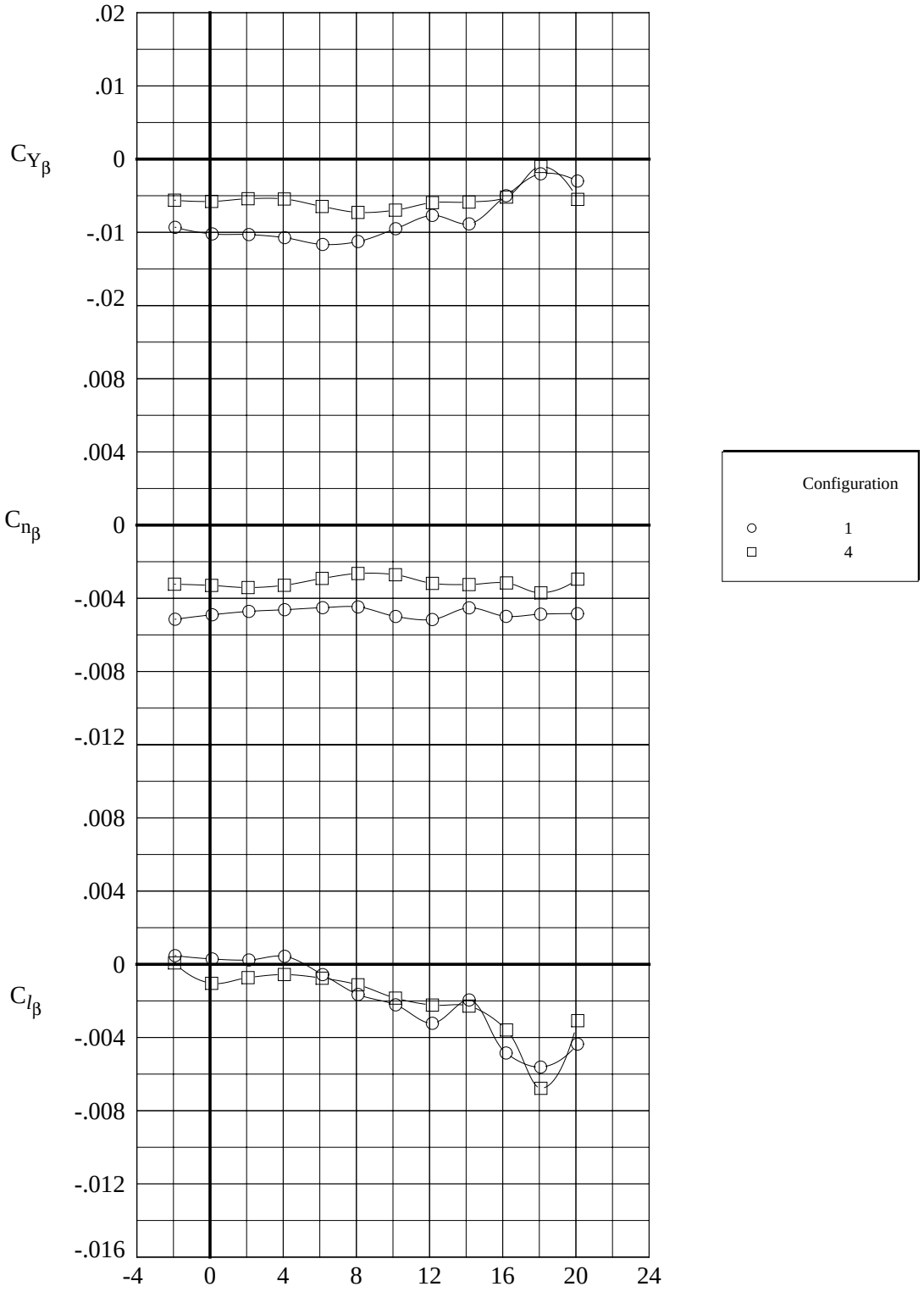


(b) $M_\infty = 0.6$

Figure 11. Concluded.

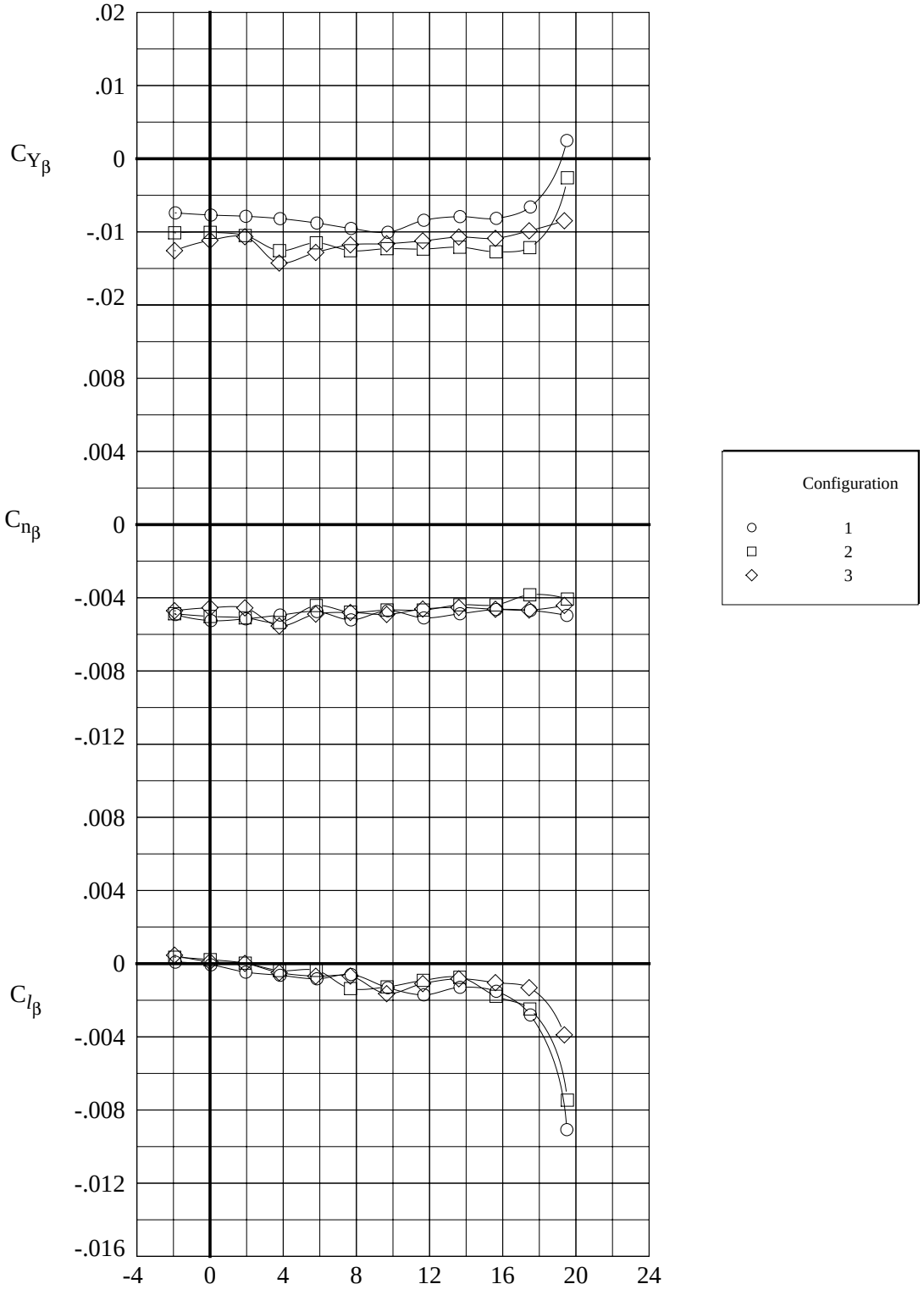


(a) $M_\infty = 0.3$

Figure 12. Effect of boattails on the lateral-directional aerodynamic characteristics of the AMLS orbiter.

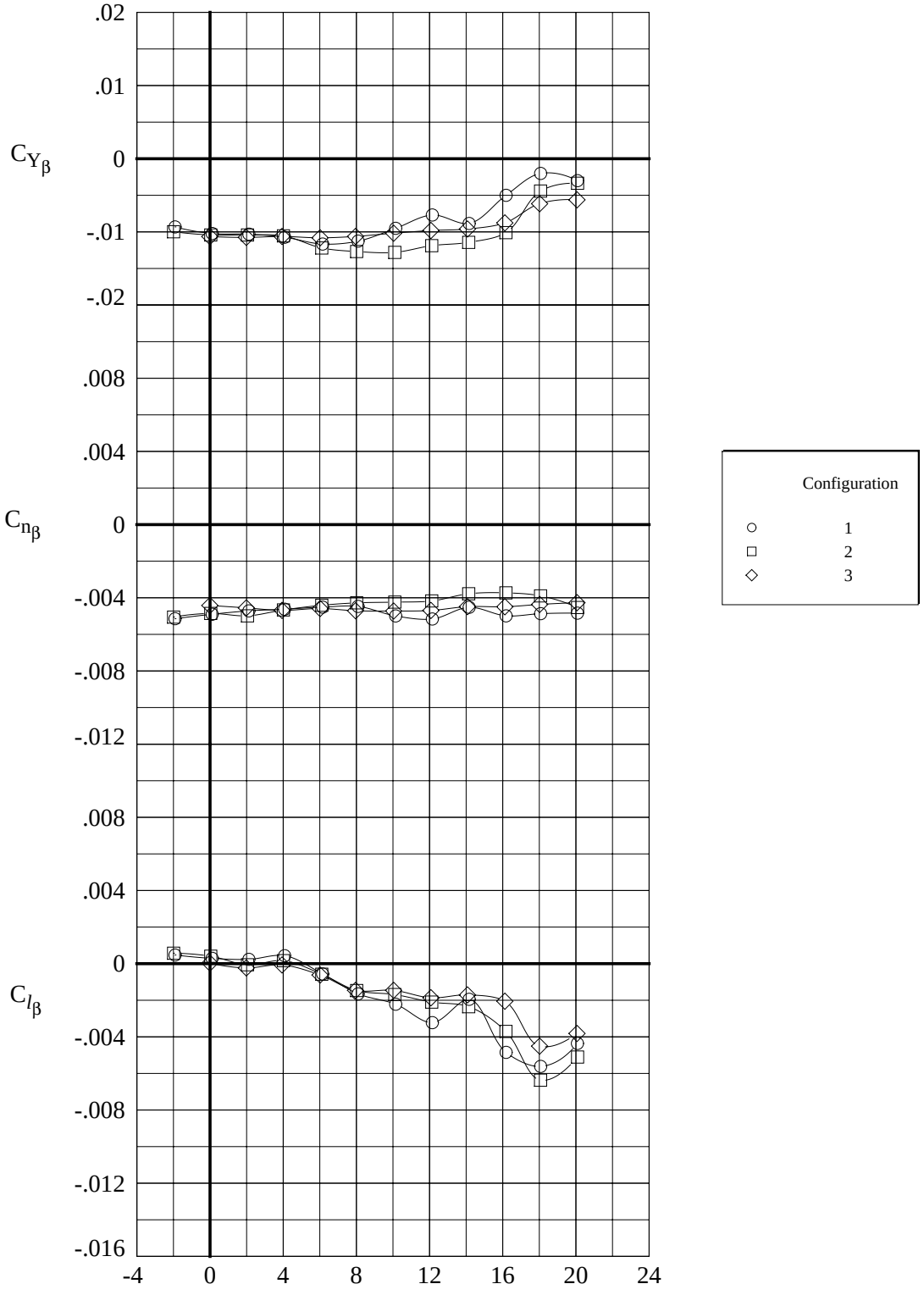


(b) $M_\infty = 0.6$

Figure 12. Concluded.

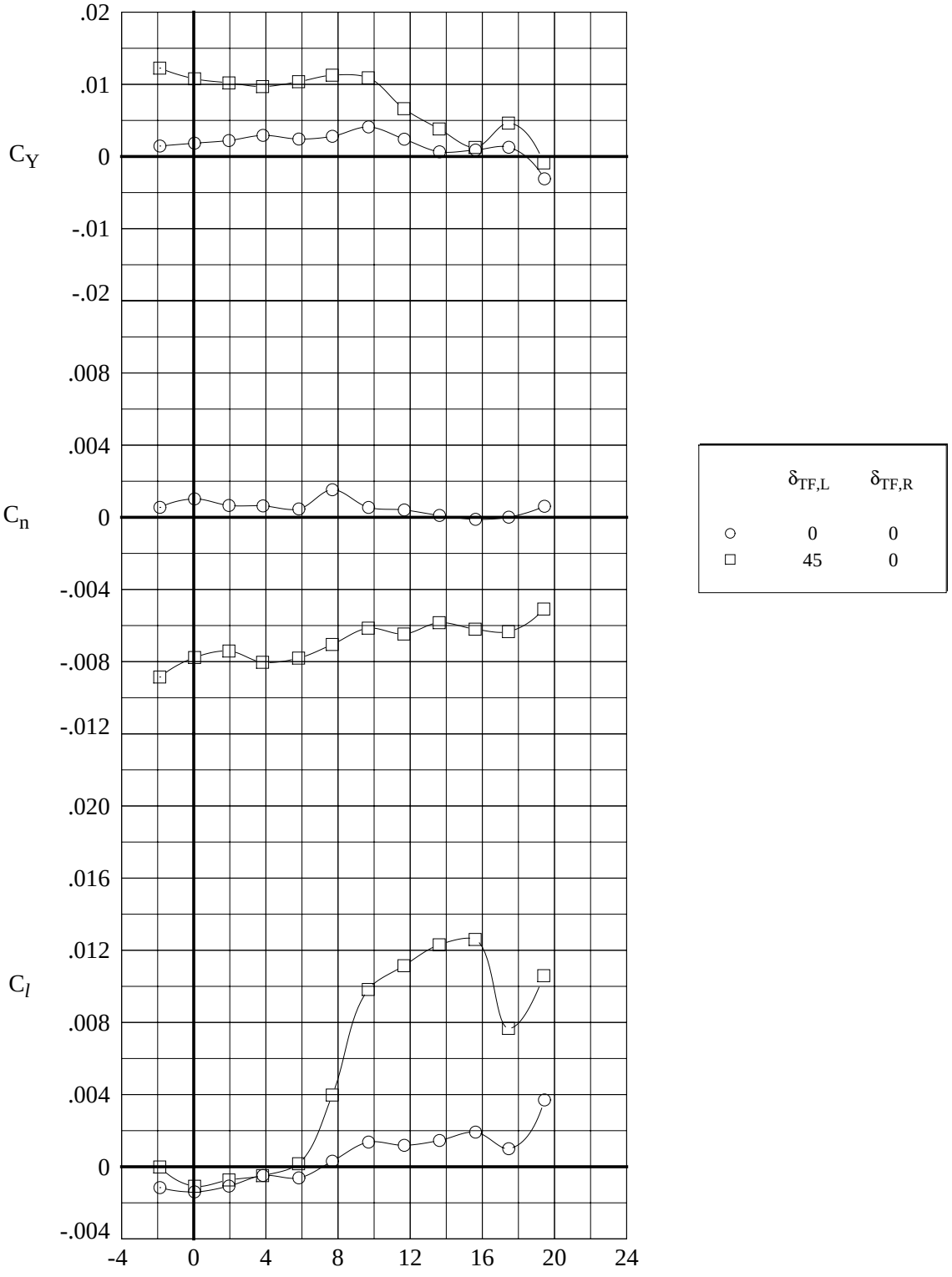


(a) $M_\infty = 0.3$

Figure 13. Effect of yaw control deflection on the lateral-directional aerodynamic characteristics of the AMLS orbiter. $\beta = 0$.

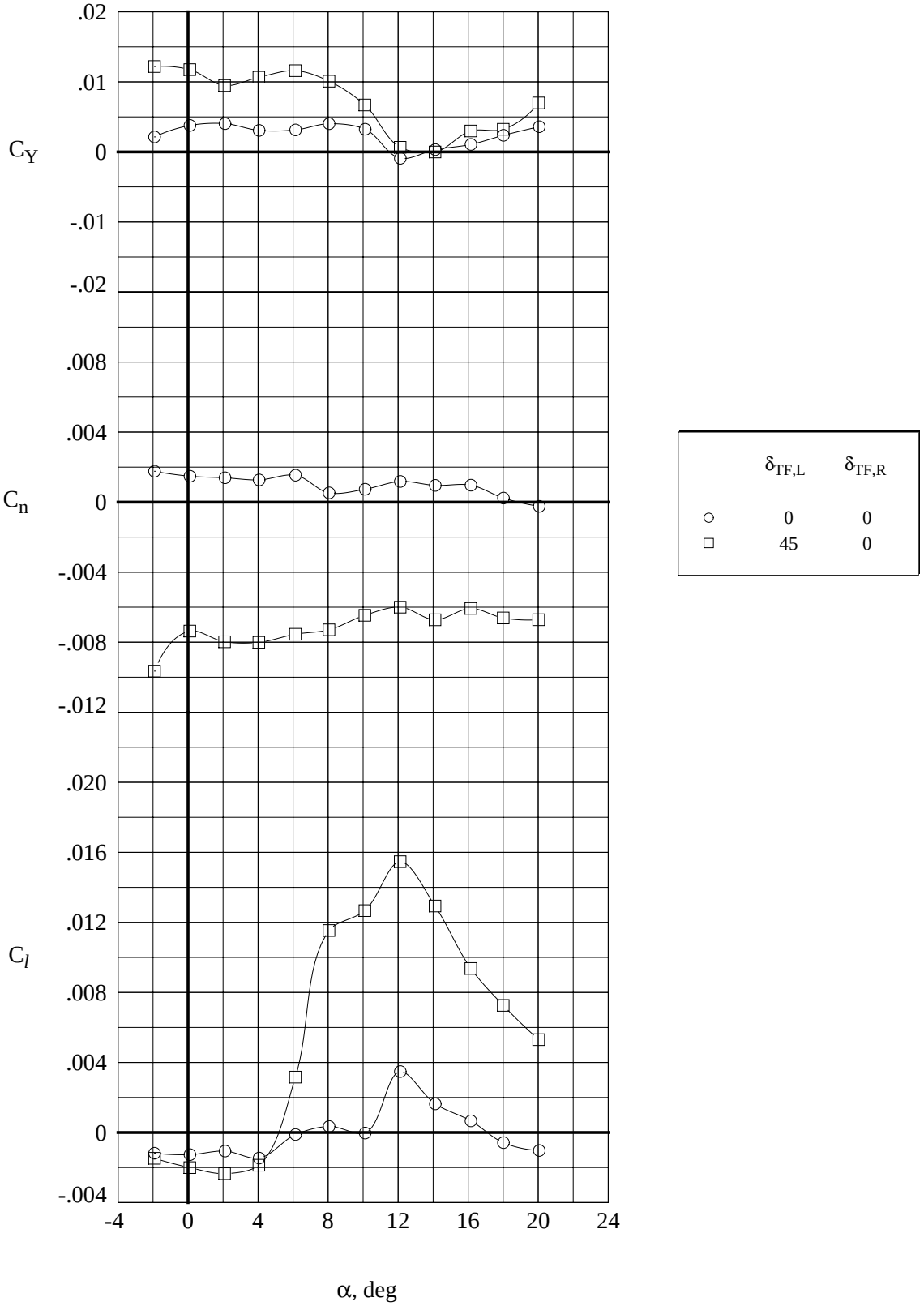


(b) $M_\infty = 0.6$

Figure 13. Concluded

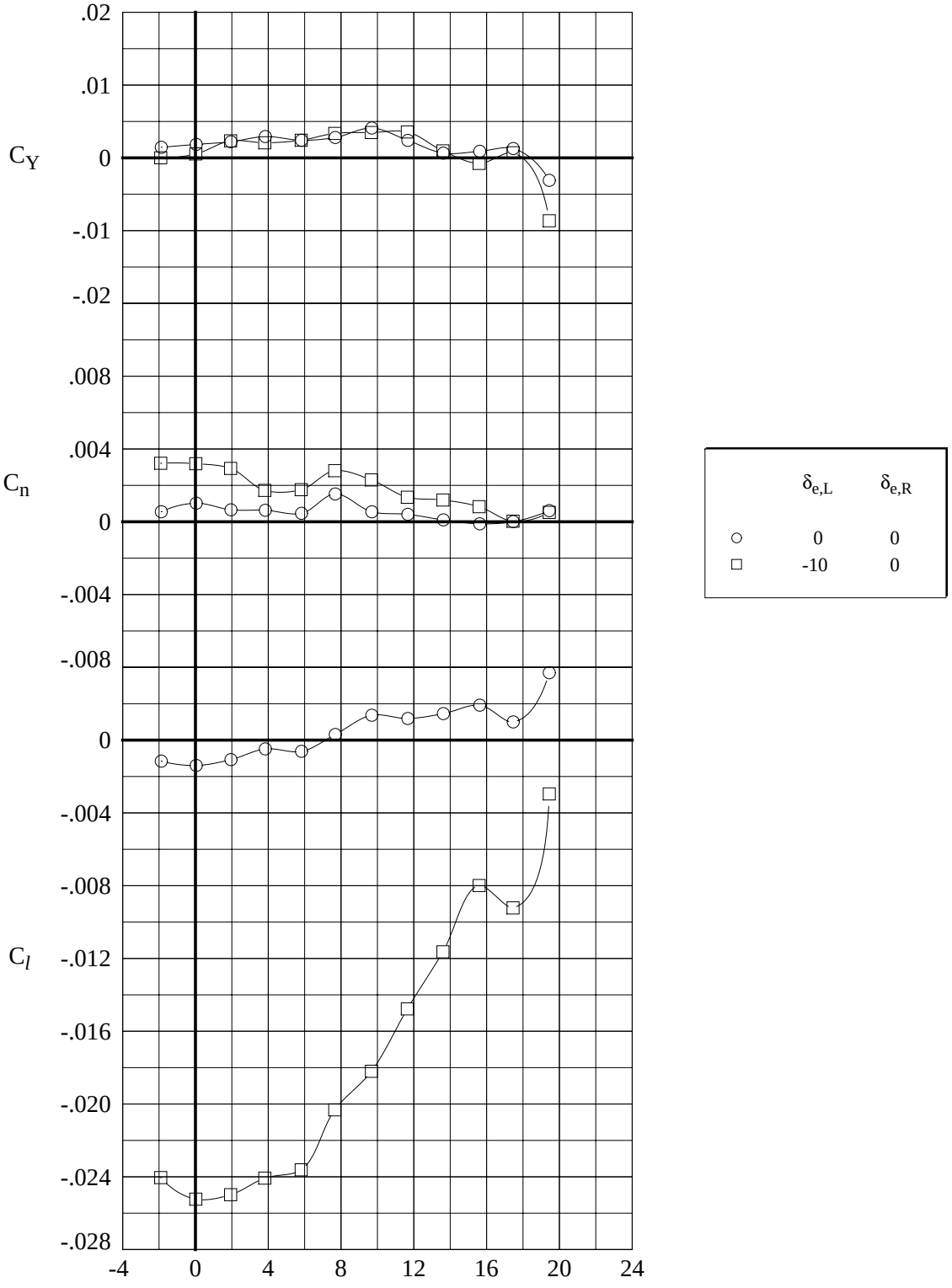


(a) $M_\infty = 0.3$

Figure 14. Effect of roll control deflection on the lateral-directional aerodynamic characteristics of the AMLS orbiter. $\beta = 0$.

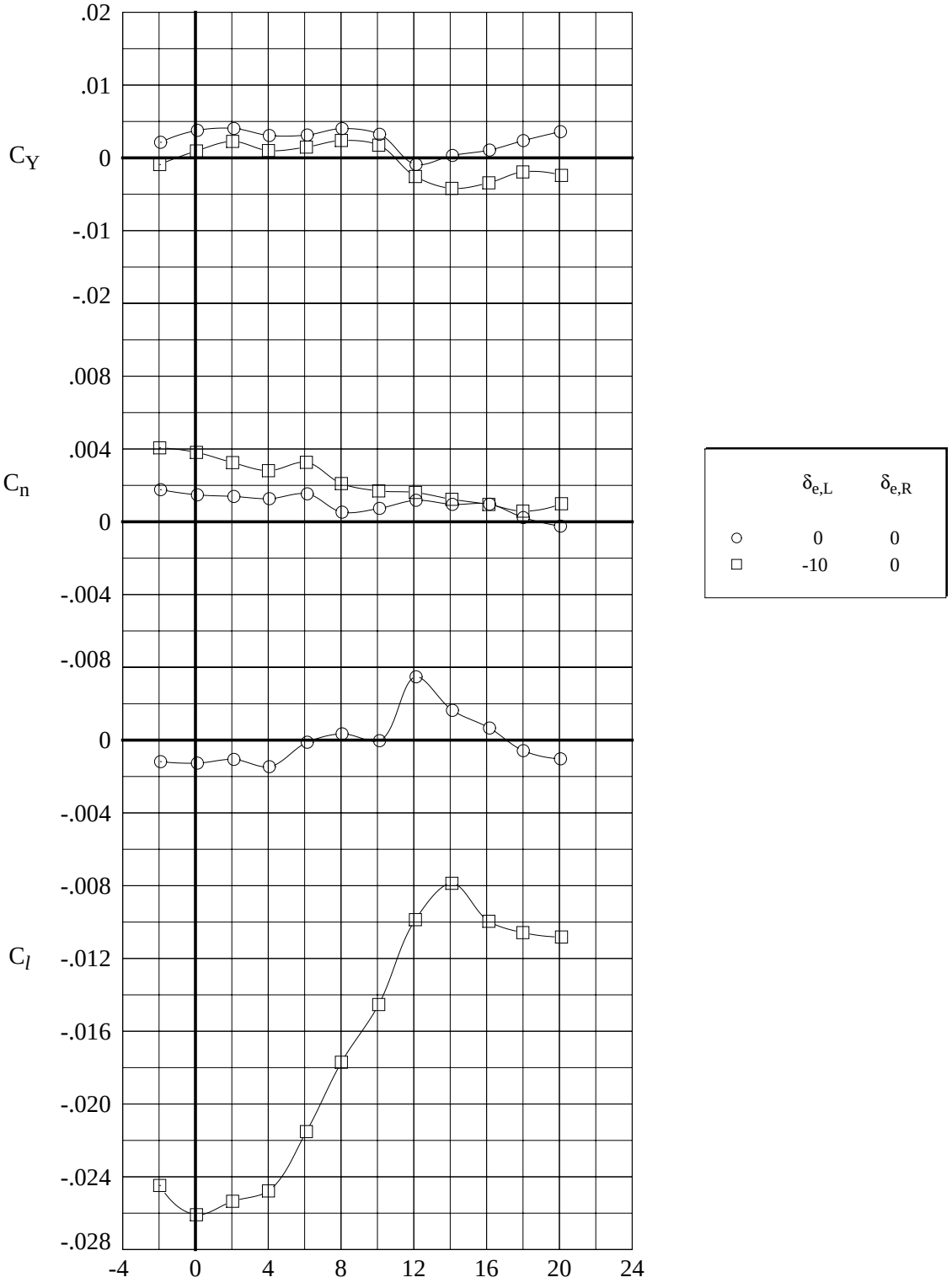


(b) $M_\infty = 0.6$

Figure 14. Concluded

# REPORT DOCUMENTATION PAGE

*Form Approved*
*OMB No. 0704-0188*



| 1. AGENCY USE ONLY *(Leave blank)* | 2. REPORT DATE | 3. REPORT TYPE AND DATES COVERED |
|---|---|---|
| | February 1993 | Technical Memorandum |

**4. TITLE AND SUBTITLE**
Subsonic Aerodynamic Characteristics of a Proposed Advanced Manned Launch System Orbiter Configuration

**5. FUNDING NUMBERS**
WU 506-40-61-01

**6. AUTHOR(S)**
George M. Ware and Charles H. Fox, Jr.

**7. PERFORMING ORGANIZATION NAME(S) AND ADDRESS(ES)**
NASA Langley Research Center
Hampton, VA 23681-0001

**8. PERFORMING ORGANIZATION REPORT NUMBER**
L-17182

**9. SPONSORING/MONITORING AGENCY NAME(S) AND ADDRESS(ES)**
National Aeronautics and Space Administration
Washington, DC 20546-0001

**10. SPONSORING/MONITORING AGENCY REPORT NUMBER**
NASA TP-4439

**11. SUPPLEMENTARY NOTES**

**12a. DISTRIBUTION/AVAILABILITY STATEMENT**
Unclassified–Unlimited

Subject Category 02

**12b. DISTRIBUTION CODE**

**13. ABSTRACT** *(Maximum 200 words)*

The Advanced Manned Launch System is a proposed near-term technology, two-stage, fully reusable launch system that consists of an unmanned glide-back booster and a manned orbiter. An orbiter model that featured a large fuselage and an aft delta wing with tip fins was tested in the Langley 7- by 10-Foot High-Speed Tunnel. A crew cabin, large payload fairing, and crew access tunnel were mounted on the upper body. The results of the investigation indicated that the configuration was longitudinally stable to an angle of attack of about 6° about a center-of-gravity position of 0.7 body length. The model had an untrimmed lift-drag ratio of 6.6, but could not be trimmed at positive lift. The orbiter model was also directionally unstable. The payload fairing was responsible for about half the instability. The tip-fin controllers, which are designed as active controls to produce artificial directional stability, were effective in producing yawing moment, but sizable adverse rolling moment occurred at angles of attack above 6°. Differential deflection of the elevon surfaces was effective in producing rolling moment with only small values of adverse yawing moment.

| 14. SUBJECT TERMS | 15. NUMBER OF PAGES |
|---|---|
| AMLS; Launch system; Spacecraft; Orbiter | 28 |
| | 16. PRICE CODE: A03 |

| 17. SECURITY CLASSIFICATION OF REPORT | 18. SECURITY CLASSIFICATION OF THIS PAGE | 19. SECURITY CLASSIFICATION OF ABSTRACT | 20. LIMITATION OF ABSTRACT |
|---|---|---|---|
| Unclassified | Unclassified | | |